Dual-Band Planar Quadrature Hybrid With Enhanced Bandwidth Response

Carlos Collado, Alfred Grau, and Franco De Flaviis

***Abstract*—This paper presents the theory, design procedure, and implementation of a dual-band planar quadrature hybrid with enhanced bandwidth. The topology of the circuit is a three-branch-line (3-BL) quadrature hybrid, which provides much larger flexibility to allocate the desired operating frequencies and necessary bandwidths than other previously published configurations. A performance comparison with other dual-band planar topologies is presented. Finally, a 3-BL quadrature hybrid for dual band (2.4 and 5 GHz) wireless local area network systems was fabricated, aimed to cover the bands corresponding to the standards IEEE802.11a/b. The measurements show a 16% and 18% bandwidth for the lower and upper frequency, respectively, satisfying and exceeding the bandwidth requirements for the above standards.**

***Index Terms*—Dual-band hybrid, planar quadrature hybrid, wireless local area network (WLAN) systems.**

I. Introduction

THE USE of circuits able to be functional at multiple frequencies is of great interest for the integration of the circuitry in systems that can operate at multiple frequency bands. Examples of those are the mobile communications systems with cellular and personal communications system (PCS) bands, and wireless local area network (WLAN) systems with multiple standards such as IEEE802.11b/g for the 2.4-GHz band and IEEE802.11a for the 5-GHz band.

One of these circuits is the target of this paper: the 90° 3-dB coupler or quadrature hybrid [1]. There are two generic approaches to achieve functionality at two frequencies f_1 and f_2, which are Δf away, either designing a broad-band hybrid whose bandwidth is greater than Δf, or designing a dual-band hybrid whose relative bandwidths (BW_1 and BW_2) at each frequency are large enough for the frequency bands assigned to the service. Broad-band hybrids can be designed either using quasi-lumped elements, usually implemented with monolithic-microwave integrated-circuit (MMIC) technology [2], [3] or enhancing the bandwidth of distributed planar elements by cascading several of them [4]. Dual-band hybrids can also be designed using several approaches. Reference [5] shows the design of a dual-band 180° hybrid using quasi-lumped elements in a microwave integrated circuit (MIC) version, [6] demonstrates the possibilities of the right-handed left-handed (RHLH) transmission lines designing a dual-band quadrature hybrid combining surface-mounted elements with planar transmission lines, [7] shows a stub loaded branch-line (BL) coupler to achieve dual-band operation, and [8] describes a dual-band two-branch-line (2-BL) coupler in which the length of one pair of parallel lines is twice longer than the length of the other pair of lines.

This study follows the line of distributed planar circuits and deals with the design of a three-branch-line (3-BL) quadrature hybrid. As we will show, the addition of a third branch to the 2-BL version gives more flexibility to allocate the frequencies of interest and provides broader bandwidths at each operation frequency at expenses of a larger size. First, we will define a basic topology of a 3-BL dual hybrid and we will describe a design procedure. An example of this basic topology was fabricated focusing on the frequencies corresponding at WLAN services and it was used as a benchmark for comparison with the dual-band planar topologies enumerated above. Finally, we show an optimized prototype of the dual hybrid with enhanced operation bandwidths for WLAN systems. The broad-band characteristics of the proposed prototype make it suitable for covering the worldwide frequencies for the 802.11b/g and 802.11a standards, in the 2.4-GHz band that extends from 2.4 to 2.49 GHz ($\mathrm{BW}_1 = 5\%$), and the 5-GHz band that extends from 5.15 to 5.825 GHz ($\mathrm{BW}_2 = 14\%$), respectively. Specifically, the measurements of this prototype show bandwidths greater than 16% for the lower and upper operation frequencies.

II. Basic 3-BL Topology

A. Description

Let us suppose a symmetric perfectly matched four-port network whose scattering matrix is

$$S = \begin{pmatrix} 0 & S_{12} & S_{13} & S_{14} \\ S_{12} & 0 & S_{14} & S_{13} \\ S_{13} & S_{14} & 0 & S_{12} \\ S_{14} & S_{13} & S_{12} & 0 \end{pmatrix}. \tag{1}$$

If the network is lossless and the following two conditions are satisfied:

$$S_{12} = 0 \tag{2}$$

$$|S_{13}| = |S_{14}| \tag{3}$$

Manuscript received February 17, 2005; revised June 15, 2005. This work was supported in part by the Ministry of Universities Research and Information Society of the Generalitat de Catalunya under the Gaspar de Portola 2004 Program, under Balsells Fellowships, under the California–Catalonia Engineering Innovation Program 2004, and by the National Science Foundation under Award ECS-0424454.

C. Collado is with the Department of Signal Theory and Communications, Technical University of Catalonia, Barcelona 08034, Spain (e-mail: collado@tsc.upc.edu).

A. Grau and F. De Flaviis are with the Electrical Engineering and Computer Science Department, University of California at Irvine, Irvine, CA 92697 USA (e-mail: agrau@uci.edu; franco@uci.edu).

Digital Object Identifier 10.1109/TMTT.2005.860306

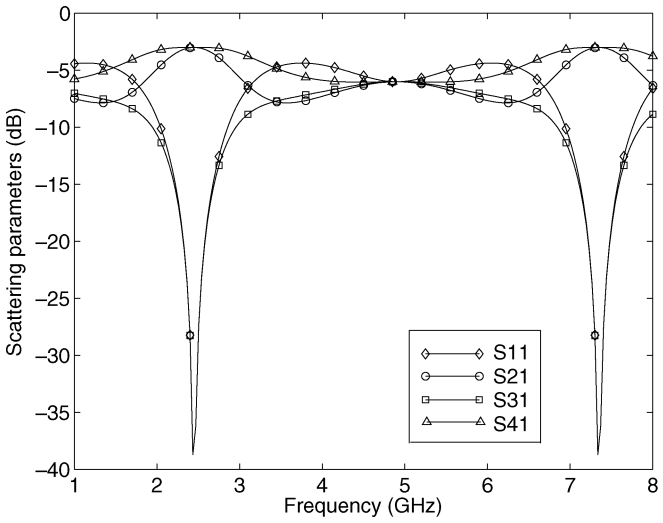

Fig. 1. S-parameters (S_{11}, S_{21}, S_{31}, and S_{41}) of a conventional BL hybrid.

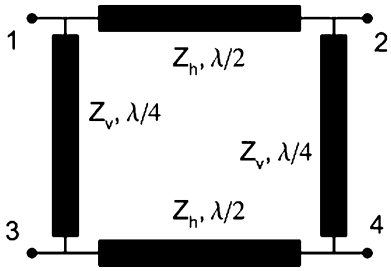

Fig. 2. Scheme of a stretched 2-BL hybrid.

this symmetric four-port network is a perfect -3-dB coupler with $|S_{13}| = |S_{14}| = 1/\sqrt{2}$ [9]. Furthermore, if the phase reference of one port is fixed, for instance, the phase of S_{13} equals zero, then

$$\varphi = \frac{\pi}{2} + n\pi \tag{4}$$

where φ is the phase of S_{14} and $n = 0, 1$ [9].

In a dual-band operation, (2) and (3) has to hold at two different and uncorrelated frequencies. The conventional BL hybrid acts as a hybrid at those frequencies f_1 and f_2, at which the BL lengths are $\lambda_1/4$ and $3\lambda_1/4$, respectively, with λ_1 being the effective wavelength at f_1 (see Fig. 1), i.e., if f_1 verifies (1), then $f_2 = 3f_1$ also does. This lack of flexibility to make f_2 independent of f_1 can be partially avoided using the stretched 2-BL hybrid described in [8] and drawn in Fig. 2. If the characteristic impedances of the lines are conveniently chosen, this stretched BL coupler will verify (2) and (3) at two frequencies that are placed symmetrically around a central frequency f_0. At f_0, the lengths of the longer pair of parallel lines are $\lambda_0/2$ and the lengths of the shorter lines are $\lambda_0/4$.

As an example, Fig. 3 shows the scattering parameters of a dual 2-BL hybrid. The two frequencies at which condition (2) is fulfilled are clearly identified and changes in the characteristic impedances of the lines would allow to move the relative position of f_1 and f_2 with respect to the central frequency f_0 [8].

The bandwidths of the lower and higher frequency bands BW_1 and BW_2, defined by a deviation of 0.5 dB in the S_{13}- and S_{14}-parameters of this example are less than 10% and 5%, respectively. These values are approximately half of those that could be achieved with a conventional no-dual BL coupler, which are around 18% at f_1 and 8% at $3f_1$ (see Fig. 1). For some applications, for example WLAN systems, those bandwidths are insufficient.

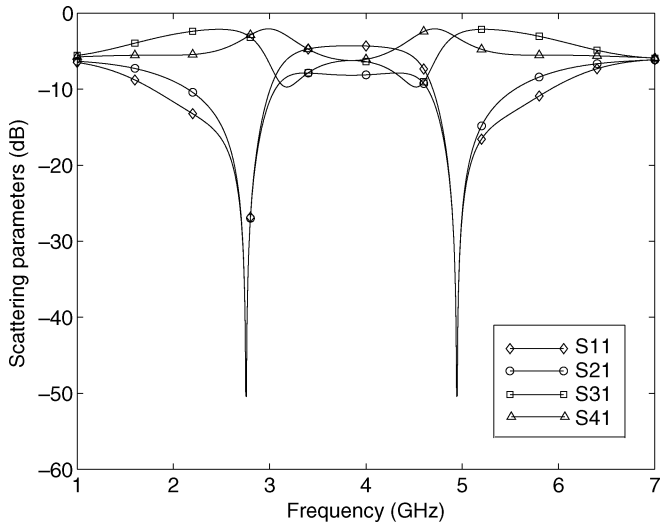

Fig. 3. S-parameters (S_{11}, S_{21}, S_{31}, and S_{41}) of the stretched 2-BL hybrid when $Z_v = 40\ \Omega$ and $Z_h = 67\ \Omega$.

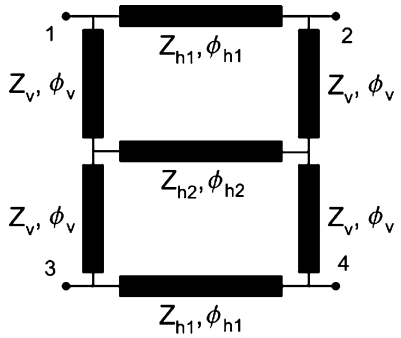

Fig. 4. Scheme of a 3-BL stretched quadrature hybrid.

In this paper, we propose a new circuit, a 3-BL coupler, shown in Fig. 4, to improve the bandwidth of this type of planar dual-band hybrids.

If conveniently designed, the S_{12} (isolated transmission path) looks like an elliptic bandpass filter response with 6 dB of insertion losses due to the matched loads at ports 3 and 4 (see Fig. 5). The central frequency (f_0) again corresponds to an electrical length of π (or physical length equals $\lambda_0/2$) for the three horizontal transmission lines, but in this case, two transmission zeros can be allocated at each band around f_0 if appropriate couplings of these three lines are achieved by appropriately designing the vertical transmission lines. The device will act as a 3-dB coupler at those frequencies where the transmission zeros are located [(2) is fulfilled] and, at the same time, (3) is satisfied. As example, Fig. 5 shows the magnitude of the scattering parameters of a dual 3-BL hybrid, and Fig. 6 shows the differential phase between its 3-dB coupled ports.

The new propagation path between ports 2 and 1, which is responsible for the additional transmission zero, introduce a new

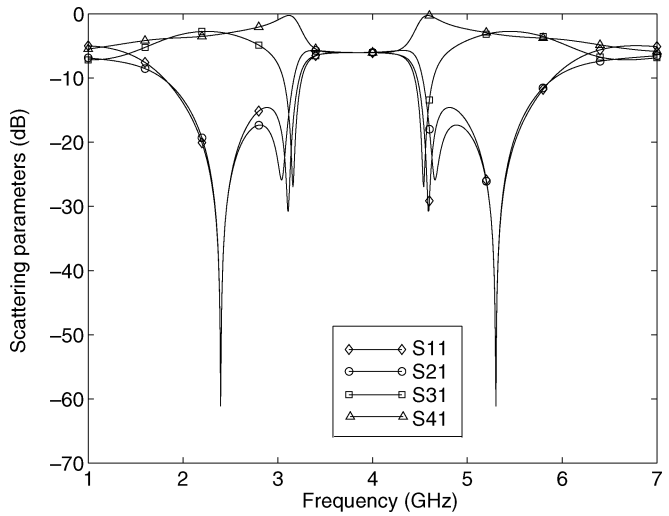

Fig. 5. S-parameters (S_{11}, S_{21}, S_{31}, and S_{41}) of a 3-BL stretched quadrature hybrid.

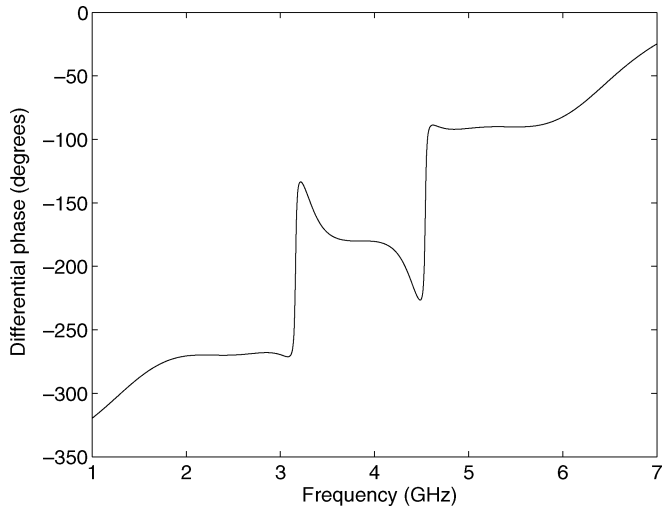

Fig. 6. Differential phase between the 3-dB coupled ports for a 3-BL stretched quadrature hybrid.

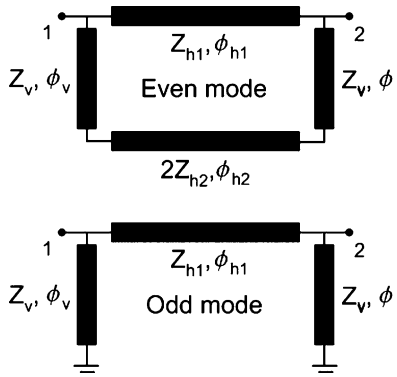

Fig. 7. Scheme of the decomposition into odd- and even-mode excitation used in analysis of the 3-BL stretched quadrature hybrid.

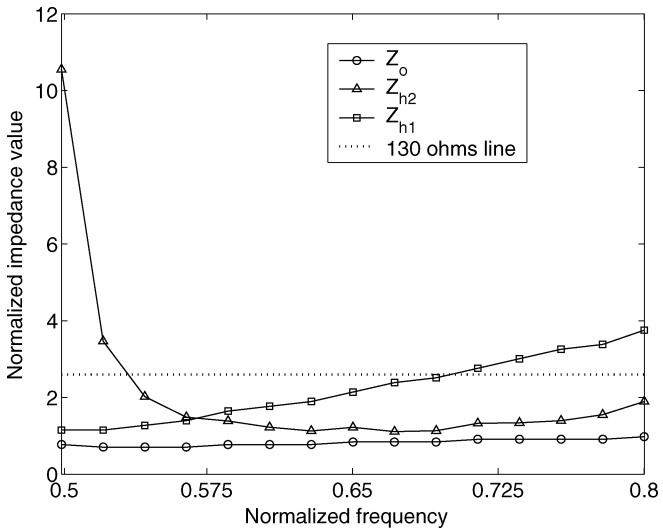

Fig. 8. Optimal impedances normalized with respect to 50 Ω: Z_{h2}, Z_{h1}, and Z_0 versus normalized frequency Ω_1. The dotted line limits the range of characteristic impedances that are usually feasible to make using microstrip lines in conventional substrates.

degree of flexibility that allows to increase the bandwidth of the coupler [10]. In particular, the example of Fig. 5 has relative bandwidths BW_1 and BW_2 around 18% and 9%, respectively, which are twice than those expected for a 2-BL version.

B. Analysis and Design

We have derived a closed-form expression for the scattering parameters as a function of the frequency for the dual 3-BL hybrid. We will follow the nomenclature outlined in Fig. 4 for the impedances and electrical lengths of the involved transmission lines (Z_v, ϕ_v, Z_{h1}, ϕ_{h1}, Z_{h2}, and ϕ_{h2}). To simplify the long formulation, we kept the electrical lengths of the horizontal lines to be equal (we will denote $\phi \equiv \phi_{h1} \equiv \phi_{h2}$) and the length of vertical lines to be half of the horizontal lines ($\phi = \phi_v/2$).

As is usually done for a symmetrical four-port network analysis, we can decompose the circuit into the superposition of an odd-mode excitation and an even-mode excitation [11]. Fig. 7 shows the equivalent circuits. Note that the transmission line at the center of the circuit (Z_{h2}, ϕ) can be split into two shunted transmission lines with impedances $2Z_{h2}$.

Besides the apparent simplicity of these equivalent circuits, the resulting scattering parameters follow long closed-form expressions (see the Appendix). These expressions cannot be simplified since, for a dual-band device, the analysis must be valid for a broad range of frequencies.

We need to find the values of ϕ, Z_v, Z_{h1}, and Z_{h2} that better satisfy the conditions of (2) and (3) at the frequencies f_1 and f_2. Using (A-1)–(A-4), it can be demonstrated that if $\phi = \pi$, the scattering parameters S_{11}, S_{12}, S_{13}, and S_{14} are -0.5, -0.5, -0.5, and 0.5, independent of the values of the characteristic impedances. This electrical length $\phi = \pi$ is the one at the central frequency f_0 of the filter-shaped response S_{12} so all the other transmission-line lengths are already fixed if we choose $f_0 = (f_1 + f_2)/2$.

Now we have to impose (2) and (3) only at the frequency f_1 since f_2 is placed symmetrical to f_1 with respect to f_0. The set of (A-1)–(A-4) can be solved numerically to find the optimum values of Z_v, Z_{h1}, and Z_{h2} for a given normalized frequency $\Omega_1 = f_1/f_0$ (see Fig. 8).

The dotted line in Fig. 8 limits the range of characteristic impedances ($< 130\ \Omega$) that could be feasible to make using microstrip lines on conventional substrates. This technological constraints fix the limits for Ω_1, i.e., $0.55 < \Omega_1 < 0.72$. The lower limit almost implies that $f_2 = 3f_1$ ($\Omega_1 = 0.5$), which is the dual response of a conventional BL hybrid, and at the upper limit, $f_1 = 0.72f_0$ implies $(f_2 - f_1)/f_0 = 0.56$, which means a bandwidth of 56%. This upper limit can be compared with the 40% bandwidth of several conventional BL hybrids connected in cascade [4] or with the 50% achievable using compensation networks at the hybrid ports [12].

We note that if optimal values of characteristic impedances are chosen according to Fig. 8, the return loss and isolation are better than 30 dB at f_1 and f_2, and the coupling values are -3 dB ± 0.1 dB.

In summary, the design procedure can be done as follows.

1) Decide the operation frequencies f_1, f_2.
2) Calculate central frequency $f_0 = (f_1 + f_2)/2$ and the normalized frequency Ω_1.
3) Choose the optimum values of Z_v, Z_{h1}, and Z_{h2} using Fig. 8.
4) Calculate the widths of the transmission lines w_v, w_{h1}, and w_{h2} according to their characteristic impedances and their corresponding lengths l_v, l_{h1}, and l_{h2} for $\phi_v \equiv \pi/2$ and $\phi_{h1} \equiv \phi_{h2} = \pi$ at f_0.

C. Fabrication Issues of Basic Dual 3-BL Hybrid

Here, we present the measurements of a benchmark dual hybrid designed using the procedure described in Section II-B. The frequencies of operation are $f_1 = 2.45$ GHz and $f_2 = 5.25$ GHz. The central frequency is then $f_0 = 3.85$ GHz and the normalized frequency is $\Omega_1 = 0.636$.

The optimal characteristic impedances can be found using Fig. 8: $Z_v = 40\,\Omega$, $Z_{h1} = 60\,\Omega$, and $Z_{h2} = 100\,\Omega$. Fig. 5 shows the S-parameters using (A-1)–(A-4). Using these formulas, theoretical bandwidths of 18% and 9% for the lower and upper band, respectively, are obtained as mentioned in Section II-A. The theoretical coupling assuming lossless transmission lines is 3 dB at f_1 and f_2.

We have fabricated this hybrid using ROGERS3006 with dielectric constant $\epsilon_r = 6.15$ and thickness $h = 0.635$ mm. The electrical parameters have been converted to physical magnitudes using LineCalc.[1] The resulting layout without an optimization procedure is shown in Fig. 9, and its physical dimensions are $w_v = 1.34$ mm, $w_{h2} = 0.66$ mm, $w_{h2} = 0.16$ mm, $l_v = 9.09$ mm, $l_{h1} = 18.80$ mm, and $l_{h2} = 19.80$ mm. The circuit fits in an area around 20 mm $\times$ 20 mm.

We have then simulated the circuit using an electromagnetic (EM) simulator to assess the discontinuity effects at the junctions between lines. At low frequencies, the simulations are in good agreement with the theoretical response using (A-1)–(A-4), while they show a decrease of the frequency around 3% (from 5.25 to 5.08 GHz) and a decrease in the bandwidth from 9% to 5% at the higher frequency band. These effects are also reproduced by the measurements as shown in Figs. 10–12 and Table I, which compares experimental results with EM simulations.

[1]Agilent Technol., Palo Alto, CA. Nov. 2004 [Online]. Available: http://www.agilent.com

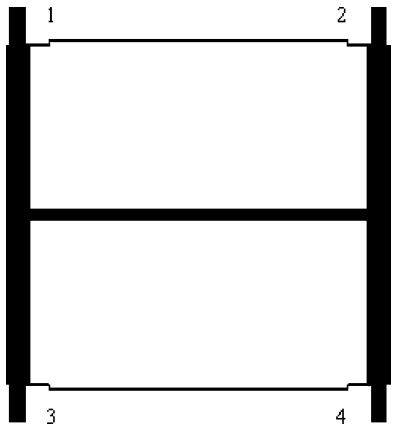

Fig. 9. Layout of the 3-BL stretched quadrature hybrid fabricated on RO3006.

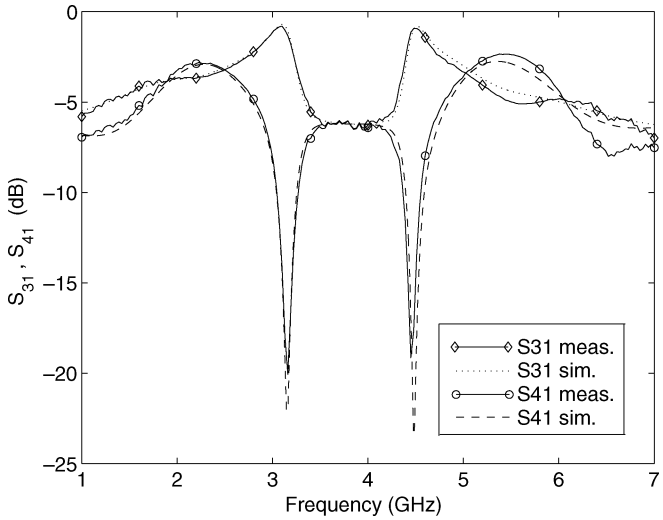

Fig. 10. Measurements and method of moments EM simulations of the S_{31}- and S_{41}-parameters of the 3-BL stretched quadrature hybrid fabricated on RO3006.

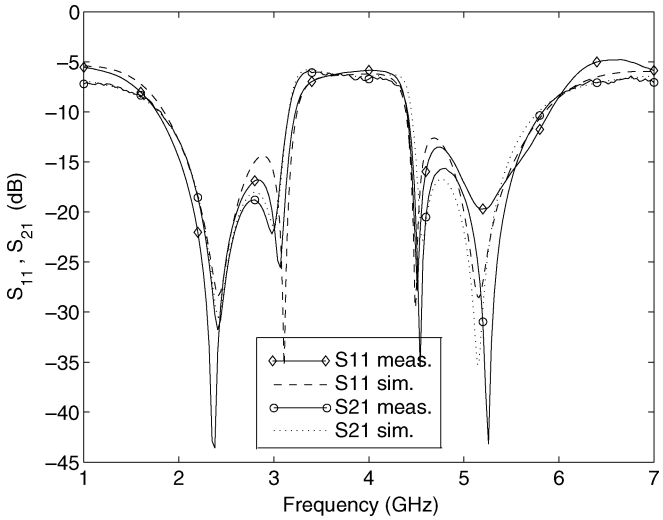

Fig. 11. Measurements (solid lines) and method of moments EM simulations of the S_{11}- and S_{21}-parameters of the 3-BL stretched quadrature hybrid fabricated on RO3006.

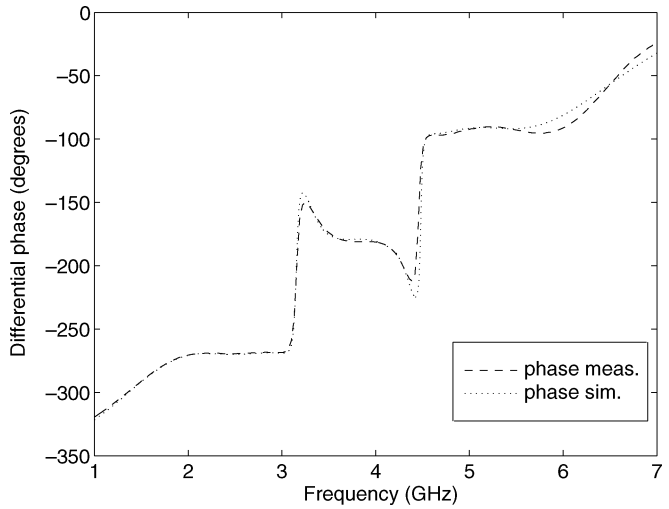

Fig. 12. Measurements and method of moments EM simulations of the differential phase between the 3-dB coupled ports of the 3-BL stretched quadrature hybrid fabricated on RO3006.

TABLE I
COMPARISON BETWEEN EXPERIMENTAL RESULTS AND EM SIMULATIONS

	Band f_1		Band f_2	
	EM sim.	Meas.	EM sim.	Meas.
Insertion loss (dB)	-3.2	-3.3	-3.3	-3.4
Isolation (dB)	-29	-28	-28	-17
ΔPhase (°)	-90	-90.6	91.2	91.8
Bandwidth (%)	20	20	5	4

As a practical point, we notice that the discontinuity effects could be diminished if the lengths of the horizontal arms are decreased by approximately 3% to compensate for the frequency-dependent response of the T junctions [13].

III. COMPARISON WITH OTHER DUAL APPROACHES

Other planar 3-dB quadrature hybrids have been simulated using the same substrate to compare them with the one presented in Section II. The goal here is to compare the performance of the basic topologies. Therefore, we will only compare the results of the simulations data obtained by a circuit simulation tool.

A. Nondual Conventional BL Hybrid

As noted in Section II-A, a nondual conventional BL coupler at 2.5 GHz presents similar insertion losses, isolation, and bandwidth that those from Table I, and its size would be 14 mm $\times$ 14 mm. Designed on ROGERS3006, the insertion losses are approximately 0.25 dB and it provides a bandwidth of 18% and 8% at f_1 and $3f_1$, respectively. Its scattering parameters can be seen in Fig. 1.

B. Dual-Band LHRH Hybrid [6]

We have designed and measured a dual hybrid using the LHRH transmissions lines proposed in [6]. The layout of the circuit is shown in Fig. 13.

Short stubs of appropriate length connected to ground through via-holes replace the shunted inductors of the RHLH lines, and the capacitors were simulated using the vendor's S-based models (Johanson 0603 model). The final design of

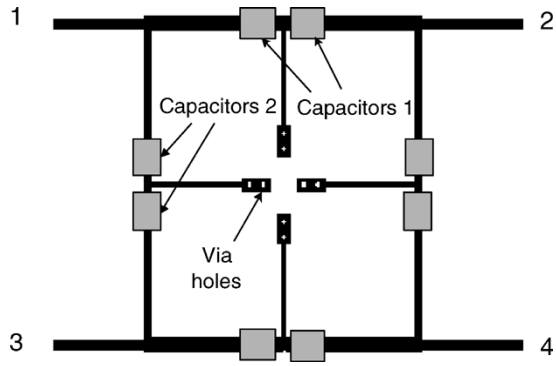

Fig. 13. Layout of the LHRH hybrid fabricated on RO3006. (1) Horizontal capacitors and (2) vertical capacitors have a capacitance value of 4.7 and 3.9 pF, respectively.

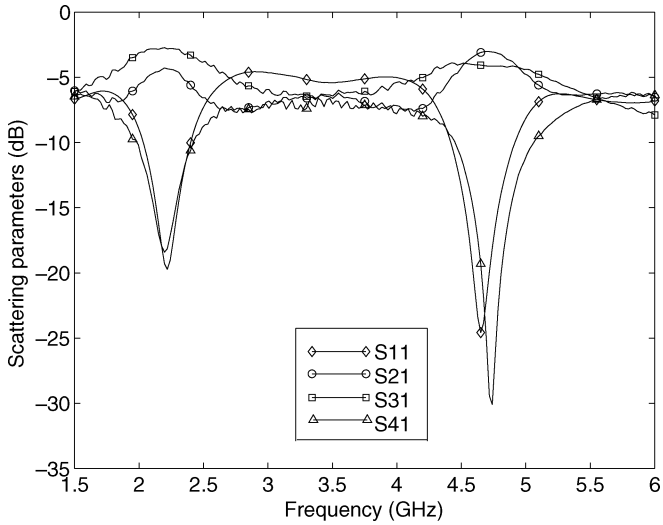

Fig. 14. Measurements of the scattering parameters of the LHRH hybrid fabricated on RO3006.

Fig. 13 was found after a process of optimization. The size of our approach was 23 mm $\times$ 26 mm. The simulations show insertion losses of 0.3 and 0.5 dB, and bandwidths around 8% and 5% for the lower and higher frequencies, respectively.

This circuit was fabricated and measured in order to verify the limits of the design due to fabrication issues, especially at high frequency, such as the self-resonant frequency and tolerance of the surface mount device (SMD) lumped components, the parasitic effects of soldering, and the via-holes. We observe similar divergences between the simulation and measurements in agreement with those commented in [6]. The lower and upper frequencies were both shifted toward lower values to 2.23 and 4.69 GHz, respectively (see Fig. 14). The amplitude imbalance between S_{31} and S_{21} was 1.64 and 1.12 dB for the lower and upper frequency, respectively. Fig. 15 shows the differential phase between the 3-dB coupled ports. As noted in [6], this approach has the inherent problems of fabrication and tuning this device and keeping the insertion losses low is a difficult task due to the complexity of the circuit.

C. Dual-Band Stub-Loaded Branch-Line (SL-BL) Hybrid

Reference [7] proposes an SL-BL hybrid to enhance the bandwidth of the dual 2-BL coupler. It can be done loading each bend

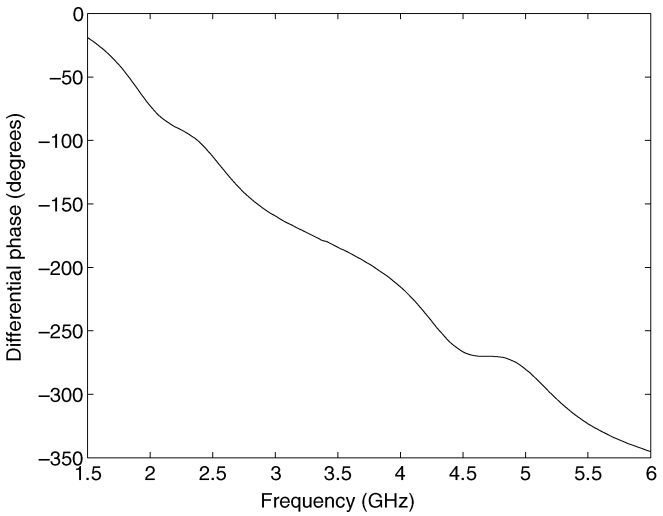

Fig. 15. Measurements of the differential phase between the 3-dB coupled ports of the LHRH hybrid fabricated on RO3006.

TABLE II
COMPARISON BETWEEN DUAL-BAND COUPLERS

	Itoh sim	2-BL sim	SL-BL sim	3-BL sim	3-BL meas
Insertion loss (dB)	0.3-0.5	0.2-0.3	0.1-0.2	0.1-0.2	0.3-0.3
Isolation (dB)	22-25	22-22	35-35	29-28	29-28
ΔPhase f_1, f_2 (°)	-90.0, 90.0	90.1, -90.1	90, 90.1	-90, 91.2	-90.6, 91.8
Bandwidth f_1-f_2 (%)	8-5	8-4	12-5.5	19-8	20-5
Size (mm)	23x26	10x20	27x10	20x20	
Complexity	High	Low	Low	Low	

of a BL coupler with an open (or shorted) stub. In this case, the simulated insertion losses are less than 0.2 dB, the isolation is better than 30 dB, and the bandwidths are 12% and 5.5% for both bands. The size is 27 mm $\times$ 9 mm.

D. Dual-Band 2-BL Hybrid

A dual 2-BL hybrid was also simulated. Its frequency response is similar than the one shown in Fig. 2. The simulated insertions losses are less than 0.2 dB, has a size of 10 mm $\times$ 20 mm, and the bandwidth are 8% and 4% for the two designed band frequencies.

E. Resume

Table II summarize the comparison between dual-band couplers. The best performances are achieved with the 3-BL coupler at expense of a higher size in comparison with the other couplers.

Finally, we have noted that the already observed better performance of the 3-BL approach can be further enhanced. If we do not impose the condition of the electrical lengths of the vertical lines being half of the length of the horizontal lines in Fig. 4, then we have an additional degree of flexibility for increasing the bandwidth of the upper band. It can be increased until 14% so that the bandwidth requirement for the IEEE802.11a WLAN standard is satisfied.

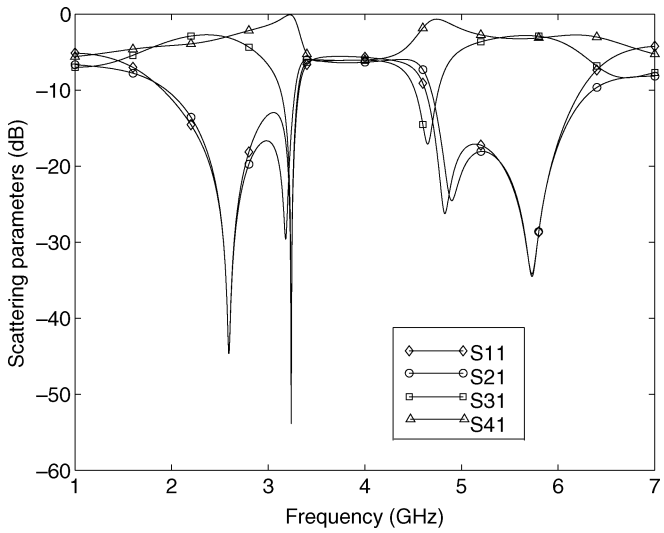

Fig. 16. S-parameters (S_{11}, S_{21}, S_{31}, and S_{41}) of a 3-BL stretched quadrature hybrid when $\phi_v = 0.85\pi/2$, and the other parameters are keep equal as in Fig. 5.

IV. HYBRID FOR WLAN SYSTEMS

The design and experimental results of a dual-band quadrature hybrid with enhanced bandwidths for WLAN systems are shown here.

The previous 3-BL hybrid was designed to satisfy (2) and (3) at the frequencies $f_1 = 2.45$ GHz and $f_2 = 5.25$ GHz, but looking at Fig. 5, we can notice that the magnitudes of S_{31} and S_{41} cross at two symmetric frequencies at each band around the central frequency. This is the key to increase the bandwidths BW_1 and BW_2, and all is needed is to impose (2) and (3) at a third frequency $f_3 = 5.8$ GHz, which is the upper limit of the higher frequency band.

As a first approach, we start using the previous dual-band design (see Fig. 5). Note that condition (3) is practically achieved at 5.8 GHz since $|S_{31}|$ and $|S_{41}|$ approximately cross at this frequency, but unfortunately, the isolation and return loss are not good enough [see condition (2)].

We need to shift the position of transmission eros at the right-hand side of f_0, but keeping constant the performance at 2.45 and 5.25 GHz. It can be achieved if we distort the symmetrical position of the zeros with respect to the central frequency and this can be done if the electrical length of the vertical lines (ϕ_v) becomes different than $\pi/2$ at the central frequency f_0. Under this condition, the formulation of the Appendix would have to be calculated again, but the addition of a new independent parameter makes the analysis quite unfeasible from a practical point-of-view.

Doing simulations, we have checked that if $\phi_v > \pi/2$, all the transmission zeros shifts to a lower frequency: lower transmission zeros move away from f_0 and the relative separation between both increase, while the zeros of the upper band moves toward f_0. On the other hand, if $\phi_v < \pi/2$, the transmission zeros moves to higher frequencies, as can be seen if we compare Fig. 5 with the simulation of Fig. 16 that was obtained with $\phi_v = 0.85(\pi/2)$ and keep equal the other parameters.

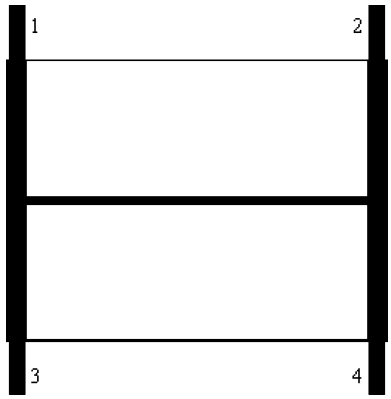

Fig. 17. Layout of the optimized hybrid for WLAN systems.

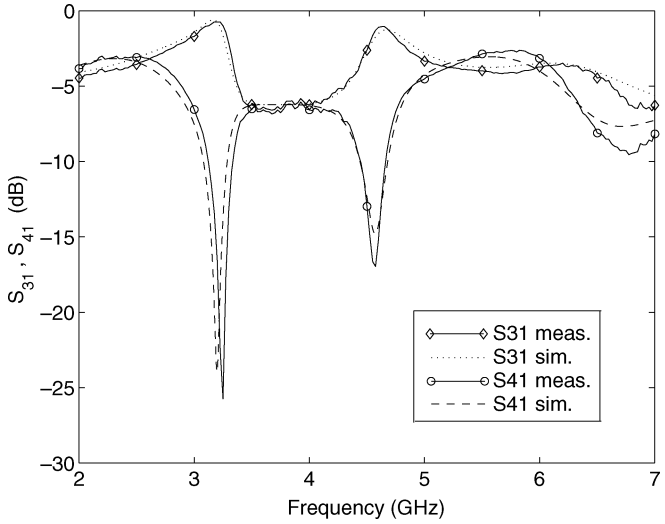

Fig. 18. Measurements and method of moments EM simulations of the S_{31}-and S_{41}-parameters of the hybrid for WLAN systems fabricated on RO3006.

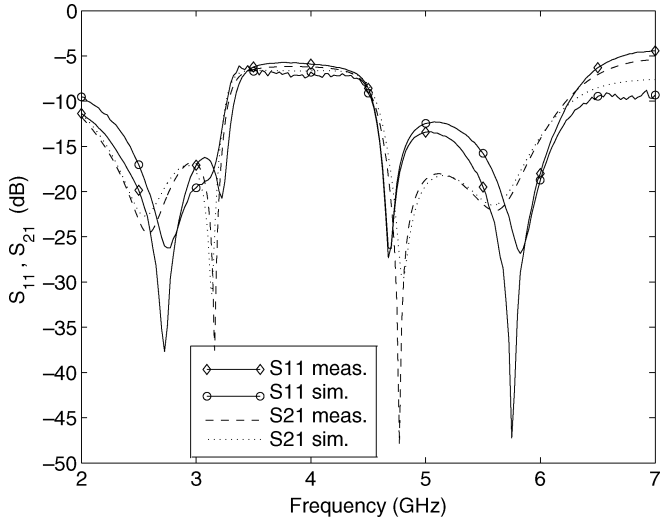

Fig. 19. Measurements and method of moments EM simulations of the S_{11}-and S_{21}-parameters of the hybrid for WLAN systems fabricated on RO3006.

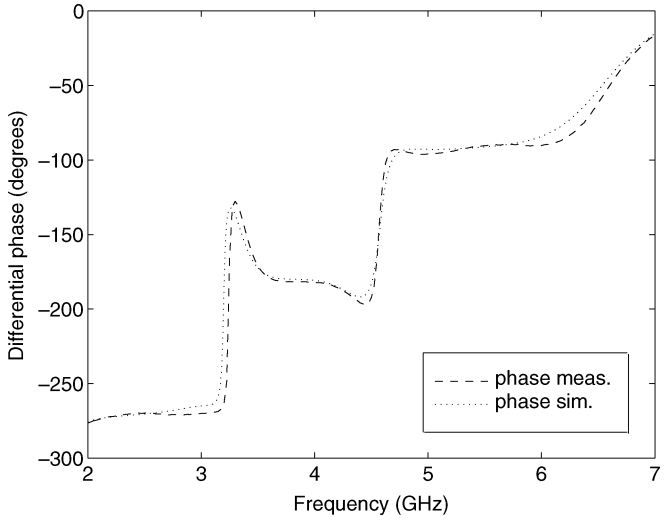

Fig. 20. Measurements and method of moments EM simulations of the differential phase between the 3-dB coupled ports of the hybrid for WLAN systems fabricated on RO3006.

We can use this ability to shift the relative position of the transmission zeros to increase BW_1 and BW_2. Moreover, we impose that the physical length of the three parallel lines is the same in order to avoid curve of the high impedances lines, as was done in the layout of Fig. 9. The final physical parameters were found by optimization of EM simulations using the basic dual 3-BL, which gives the results of Fig. 5 as a starting point.

The resulting parameters are $w_{h1} = 0.161$ mm, $w_{h2} = 0.486$ mm, $w_v = 1.114$ mm, $l_{h1} = l_{h2} = 19.45$ mm, and $l_v = 16.148$ mm; and the layout can be seen in Fig. 17, which fits into an area of 21.7 mm $\times$ 16.2 mm.

Figs. 18–20 shows the measurements and the method of moments EM simulations of the most relevant scattering parameters (S_{11}, S_{21}, S_{31}, and S_{41}) and the differential phase between the 3-dB coupled ports of the hybrid for WLAN systems fabricated on RO3006. These figures shows the good agreement between the experimental results and EM simulations, and Table III summarize the results at each frequency.

The insertion losses are quite low in spite of the narrow transmission lines. Note that the bandwidth values are $\mathrm{BW}_1 = 16\%$ and $\mathrm{BW}_2 = 18\%$, which fulfills the requirements of a dual-band hybrid for WLAN systems, although it has an imbalance response around 1 dB in the coupling values at the central frequency (~5.6 GHz) of the upper band, 0.6 dB at f_1, 0.7 dB at f_2, and 0.9 dB at f_3. This imbalance response could likely diminished if a more exhaustive optimization process is done.

TABLE III
MEASUREMENT RESULTS OF THE HYBRID FOR WLAN SYSTEMS AT EACH FREQUENCY

	f_1	f_2	f_3
Coupling (dB)	-3.3	-3.5	-3.4
Isolation (dB)	21	15	21
ΔPhase (°)	-91.2	91.0	85
Imbalance (dB)	0.6	0.7	0.9

V. SUMMARY AND CONCLUSIONS

The proposed 3-BL circuit allows to design planar dual-band quadrature hybrids in the range of normalized frequencies

$0.55 < \Omega_1 < 0.72$. This range falls into the gap that cannot be achieved with a conventional BL hybrid operating at the first and third harmonic or with the cascade of several of these hybrids [4].

Closed forms of the scattering parameters have been derived and, therefore, an easy design procedure has been outlined. Using that procedure, we have designed as benchmark circuit a dual-band 3-BL hybrid without any *a posteriori* optimization process. We have found that the experimental data is very close to the theoretical scattering parameters due to its simple layout.

This benchmark circuit has been compared with other planar dual-band hybrids proposed in the literature, showing similar performances in terms of isolation, return, and insertion losses, but with a significative improvement of the bandwidth at each operation frequency at expenses of a higher size. Furthermore, the bandwidths of this basic 3-BL hybrid can be even enhanced if the conditions imposed to the basic structure with the objective to achieve closed-form expressions for the design are relaxed.

Doing that, we have designed and measured a dual-band hybrid to be used in WLAN systems under the standards IEEE802.11a/b, which specify a minimum bandwidth of 14% for the upper band to cover the worldwide services. Bandwidths of 16% and 18% were measured for the lower and upper band, respectively, thus, the proposed circuit satisfies the requirements of those standards.

The given designs are not optimized in size. Common techniques to reduce the size of a conventional BL coupler could also be used to minimize the area of these hybrids. We are exploring these two possibilities: curve the lines, as done in [14], or using stubs loads, as done in [7] and [15].

These dual hybrids can be used in several systems. In particular, we are focusing in on the design of a Butler matrix [16] to feed antenna arrays for dual-band systems. Preliminary results have shown the feasibility of the proposed circuit and the results will be published in future papers.

APPENDIX I
FORMULATION OF THE SCATTERING PARAMETERS FOR THE 3-BL STRETCHED QUADRATURE HYBRID

$$S_{11} = \frac{1}{2}\rho_e + \frac{1}{2}\rho_o \tag{A-1}$$

$$S_{13} = \frac{1}{2}\tau_e + \frac{1}{2}\tau_o \tag{A-2}$$

$$S_{14} = \frac{1}{2}\tau_e - \frac{1}{2}\tau_o \tag{A-3}$$

$$S_{22} = \frac{1}{2}\rho_e - \frac{1}{2}\rho_o \tag{A-4}$$

$$\rho_o = \frac{A_o + B_o}{C_o - A_o + B_o} \tag{A-5}$$

$$\tau_o = \frac{2}{C_o - A_o + B_o} \tag{A-6}$$

$$\rho_e = \frac{A_e - B_e}{A_e + B_e + C_e} \tag{A-7}$$

$$\tau_e = \frac{2}{A_e + B_e + C_e} \tag{A-8}$$

and (A-9)–(A14), shown at the bottom of this page.

ACKNOWLEDGMENT

Author C. Collado wishes to thank the Ministry of Universities Research and Information Society (DURSI) of the General-

$$A_o = \frac{iZ_{0_{\text{port}}}(Z_0+Z_2)\big(-Z_0+Z_2+(Z_0+Z_2)\cos(\phi)\big)\cot\left(\frac{\phi}{2}\right)}{Z_0^2 Z_2} \tag{A-9}$$

$$B_o = \frac{2\big(Z_2+(Z_0+Z_2)\cos(\phi)\big)}{Z_0} \tag{A-10}$$

$$C_o = \frac{iZ_2\sin(\phi)}{Z_{0_{\text{port}}}} \tag{A-11}$$

$$A_e = \frac{i\sin(\phi)}{Z_{0_{\text{port}}}\left(\dfrac{1}{Z_2} + \dfrac{4Z_1}{(Z_0+2Z_1)\big(-Z_0+2Z_1+(Z_0+2Z_1)\cos(\phi)\big)}\right)} \tag{A-12}$$

$$B_e = \frac{-2Z_0\left(Z_0^2-4Z_1^2\right)\cos(\phi) + 2Z_0(Z_0+2Z_1)^2\cos(\phi)^2 + Z_2\left(-(Z_0-2Z_1)^2+(Z_0+2Z_1)^2\cos(2\phi)\right)}{Z_0\left(-Z_0^2+4Z_1(Z_1+Z_2)+(Z_0+2Z_1)^2\cos(2\phi)\right)} \tag{A-13}$$

$$C_e = \frac{iZ_{0_{\text{port}}}\left(-Z_0^4+4Z_0^3Z_1+12Z_0^2Z_1^2+2Z_0^3Z_2+24Z_0^2Z_1Z_2+8Z_0Z_1^2Z_2+3Z_0^2Z_2^2+4Z_0Z_1Z_2^2-4Z_1^2Z_2^2\right)\tan\left(\frac{\phi}{2}\right)}{2Z_0^2Z_2\left(-Z_0^2+4Z_1(Z_1+Z_2)+(Z_0+2Z_1)^2\cos(\phi)\right)}$$
$$+\frac{iZ_{0_{\text{port}}}\left(4Z_0(Z_0+2Z_1)(Z_0+Z_2)(2Z_1+Z_2)\cos(\phi)+(Z_0+2Z_1)^2(Z_0+Z_2)^2\cos(2\phi)\right)\tan\left(\frac{\phi}{2}\right)}{2Z_0^2Z_2\left(-Z_0^2+4Z_1(Z_1+Z_2)+(Z_0+2Z_1)^2\cos(\phi)\right)} \tag{A-14}$$

itat de Catalunya for hosting him at the Electrical Engineering and Computer Science Department, University of California at Irvine.

REFERENCES

[1] L. Young, "Synchronous branch guide directional couplers for low and high power applications," *IEEE Trans. Microw. Theory Tech.*, vol. MTT-10, no. 11, pp. 459–475, Nov. 1962.

[2] T. Kawai, Y. Kokubo, and I. Ohta, "Broadband lumped-element 180-degree hybrids utilizing lattice circuits," in *IEEE MTT-S Int. Microwave Symp. Dig.*, vol. 1, May 2001, pp. 47–50.

[3] F. Ali and A. Podell, "A wide-band GaAs monolithic spiral quadrature hybrid and its circuit applications," *IEEE J. Solid-State Circuits*, vol. 26, no. 10, pp. 1394–1398, Oct. 1991.

[4] M. Muraguchi, T. Yukitake, and Y. Naito, "Optimum design of 3 dB branch-line couplers using microstrip lines," *IEEE Trans. Microw. Theory Tech.*, vol. MTT-83, no. 8, pp. 674–678, Aug. 1983.

[5] F. Giannini and L. Scucchia, "A double frequency 180° lumped-element hybrid," *Microwave Opt. Technol. Lett.*, vol. 33, no. 4, pp. 247–251, May 2002.

[6] I.-H. Lin, M. DeVincentis, C. Caloz, and T. Itoh, "Arbitrary dual-band components using composite right/left-handed transmission lines," *IEEE Trans. Microw. Theory Tech.*, vol. MTT-4, no. 10, pp. 246–252, Oct. 1956.

[7] K.-K. M. Cheng and F.-L. Wong, "A novel approach to the design and implementation of dual-band compact planar 90° branch-line coupler," *IEEE Trans. Microw. Theory Tech.*, vol. 52, no. 11, pp. 2458–2463, Nov. 2004.

[8] F.-L. Wong and K.-K. M. Cheng, "A novel planar branch-line coupler design for dual-band applications," in *IEEE MTT-S Int. Microwave Symp. Dig.*, vol. 2, Jun. 2004, pp. 903–906.

[9] D. M. Pozar, *Microwave Engineering*, 2nd ed. New York: Wiley, 1998.

[10] T. Q. Wang and K. Wu, "Size-reduction and band-broadening design technique of uniplanar hybrid ring coupler using phase inverter for M(H)MICs," *IEEE Trans. Microw. Theory Tech.*, vol. 47, no. 2, pp. 198–206, Feb. 1999.

[11] J. Reed and G. J. Wheeler, "A method of analysis of symmetrical four-port networks," *IEEE Trans. Microw. Theory Tech.*, vol. MTT-4, no. 10, pp. 246–252, Oct. 1956.

[12] R. Knochel, "Broadband flat coupling two-branch and multibranch directional couplers," in *IEEE MTT-S Int. Microwave Symp. Dig.*, vol. 3, Jun. 1999, pp. 1327–1330.

[13] W. Menzel and I. Wolff, "A method for calculating the frequency-dependent properties of microstrip discontinuities," *IEEE Trans. Microw. Theory Tech.*, vol. MTT-25, no. 2, pp. 107–112, Feb. 1977.

[14] A. Corona and M. J. Lancaster, "A high-temperature superconducting butler matrix," *IEEE Trans. Appl. Supercond.*, vol. 13, no. 12, pp. 3867–3872, Dec. 2003.

[15] T. Hirota, A. Minakawa, and M. Muraguchi, "Reduced-size branch-line and rat-race hybrids for uniplanar MMIC's," *IEEE Trans. Microw. Theory Tech.*, vol. 38, no. 11, pp. 270–275, Nov. 1990.

[16] J. Butler and R. Lowe, "Beam forming matrix simplifies design of electronically scanned antennas," *IEEE Trans. Appl. Supercond.*, vol. AC-9, no. 4, pp. 170–173, Apr. 1961.

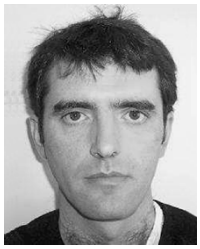

Carlos Collado was born in Barcelona, Spain, in 1969. He received the Telecommunication engineering and Ph.D. degrees from the Universitat Politècnica de Catalunya (UPC), Barcelona, Spain, in 1995 and 2001 respectively, and the Master degree in bioengineering from the Centre de Recerca en Enginyeria Biomdica (UPC), Barcelona, Spain, in 2002.

He is currently an Associate Professor with UPC, where he teaches courses on the theory of electromagnetism, microwave laboratory, and high-frequency devices. His research interests include microwave devices and systems, including high-frequency applications of superconductors.

Alfred Grau was born in Barcelona, Spain, in 1977. He received the Telecommunication Engineer degree from the Universitat Politècnica de Catalunya (UPC), Barcelona, Spain, in 2001, the M.S. degree from the University of California at Irvine (UCI), in 2004, and is currently working toward the Ph.D. degree at UCI.

His current research is focused on small antennas, multielement antenna (MEA) systems, and system reconfiguration with microelectromechanical systems (MEMS).

Franco De Flaviis, was born in Teramo, Italy, in 1963. He received the Laurea degree in electronics engineering from the University of Ancona, Ancona, Italy, in 1990, and the M.S. and Ph.D. degrees in electrical engineering from the University of California at Los Angeles (UCLA), in 1994 and 1997 respectively.

In 1991, he was an Engineer with Alcatel, where he specialized in the research of microwave mixer design. In 1992, he was Visiting Researcher with UCLA, where he was involved with low-intermodulation mixers. He is currently an Associate Professor with the Department of Electrical and Computer Engineering, University of California at Irvine (UCI). His research interests are in the field of computer-aided electromagnetics for high-speed digital circuits and antennas and microelectromechanical systems (MEMS) for RF applications fabricated on unconventional substrates such as printed circuit boards and microwave laminates.